Design of Bird-Like Airfoils

Gavin K. Ananda[*] and Michael S. Selig[†]

Department of Aerospace Engineering, University of Illinois at Urbana–Champaign, Urbana, IL 61801, USA

The size constraints and high payload requirements of Micro Air Vehicles necessitate the design of vehicles with high wing loading that require efficient flight at high lift coefficients. MAVs operate in the low Reynolds number regime that is characterized by highly viscous phenomena like the laminar separation bubble causing large losses in efficiency. Drawing inspiration from nature, bird-like sectional profile airfoil families were designed in PROFOIL to operate at these Reynolds numbers. In this paper, parametric studies using multipoint inverse airfoil design are presented to demonstrate techniques and design philosophies employed to design airfoil families between 4–6% thickness that include moment constraints ranging from $C_{m,c/4}$ of -0.14 to -0.26.

I. Introduction

Nature's success in achieving flight inspired humans to seek the air. As a result, early aircraft designs mimicked avian flight, especially in its planform, use of thin airfoils, and use wing warping for control.[1] However, as the understanding of the physics of flight improved, through theoretical and experimental developments, and with expanded payload and speed requirements, the field of aircraft design diverged from its biologically inspired roots. As noted by McMasters,[2] there exists a need for bringing the two ends of the spectrum (technological and biological flight) closer in that avian flight should motivate the development of new flight technology. Bio-inspired flight vehicle design has become possible in recent years[3] with the advent of small-scale electronics and avionics that have propelled the development of small-scale unmanned aerial vehicles and micro air vehicles (MAVs). Thus, there is an increasing need to better understand avian flight that operates in the low Reynolds numbers regime (10^4–10^5).[4] It is commonly known that in this regime, highly viscous related phenomena such as the laminar separation bubble start to dominate thereby causing losses in efficiency for the airfoil. Much can still be learnt from avian flight in how biology deals with these low Reynolds number effects.

A typical bird wing produces lift, drag, and thrust through the manipulation of its planform shape, profile, and morphology.[5] For example, swift wings have the ability to increase sweep to achieve lower drag (high speed dash) and extend its wings to achieve higher lift (low speed flight/landing).[6] In addition to wing planform and morphing, the feathers of a bird play a critical role of achieving the airfoil-like cross-sections required for efficient flight. Studies have shown that although avian literature has paid less attention to airfoil sectional characteristics, the leading edge geometry, camber, and wing thickness critically affect the overall force generation of bird wings.[7] To better understand the wings of birds in its production of aerodynamic forces, detailed wing geometry measurements using 3-D scanning techniques were performed to extract properties such as planform shape, camber distribution, thickness distribution, twist distribution, and chord distribution.[8–12] The main observations from these measurements was that most bird airfoils were highly cambered in nature, had a thin aft region, and a thick leading edge. A selection of bird airfoil thickness and cambers ratios extracted from literature[8,10,11] are plotted in Fig. 1

The goal of this paper is to design a family of bird-inspired airfoils that perform efficiently at the same Reynolds number scales (10^4–10^5) and that are both thin and highly cambered in a bid to further the field of biologically-inspired micro flight. Through a systematic design approach using the PROFOIL multipoint

---

*Graduate Student (Ph.D. Candidate), 104 S. Wright St., anandak1@illinois.edu
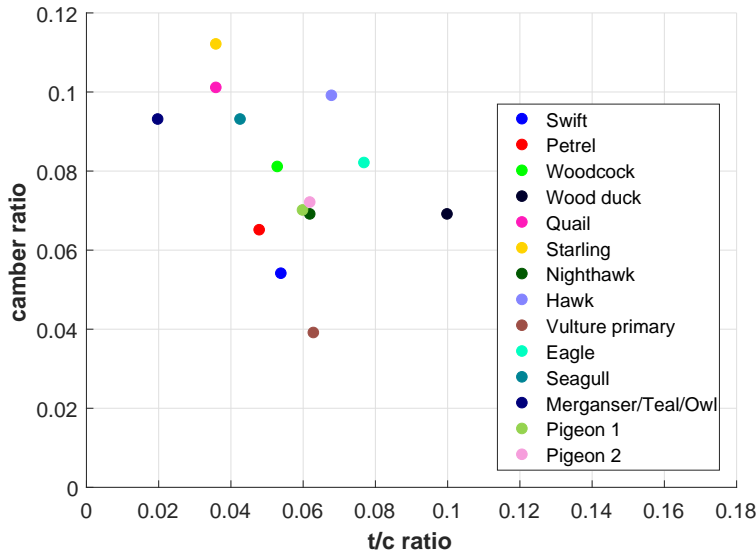†Professor, 104 S. Wright St., m-selig@illinois.edu

Figure 1. Extracted camber and thickness ratio characteristics of actual bird airfoil sections.[8,10,11]

inverse design tool,[13–16] three different families of airfoils based on moment constraints ranging from $C_{m,c/4}$ of -0.14 to -0.26 were designed. The thicknesses within each airfoil family were maintained to between 4–6%. These values were chosen as they allowed for the thickness and camber ratios of the designed airfoils to be within the limits set from actual bird airfoil cross-sections found in literature (see Fig. 1). The design approach and tools used are first discussed. Then, a detailed description of the design requirements is presented together with the designed airfoils and the associated aerodynamic performance details. Finally, a tabulated set of airfoil coordinates for each airfoil is provided in Appendix A.

II.   Approach

The general approach to designing the bird-inspired airfoils was to use the inverse airfoil design tool, PROFOIL,[13–16] together with the airfoil analysis tool, XFOIL.[17,18] PROFOIL is a multi-point inverse design tool that allows for the specification of desired velocity distributions over various segments of the airfoil along with specific constraints such as maximum thickness, enclosed area, pitching moment, and boundary layer specifications. The various design specifications result in a system of nonlinear equations that are solved using a multidimensional Newton iteration scheme. To prescribe a desired velocity distribution, the airfoil is first divided into segments. Then, using the method of conformal mapping, the arc limits ϕ on the circle are mapped to the segments s on the airfoil as shown in Fig. 2. A design angle of attack α^* is associated with each segment, where at that angle of attack, the velocity distribution along the segment will be prescribed, typically being constant as used in the current designs.

As elaborated in detail in Ref. 16, at low Reynolds numbers, the C_l–x_{tr}/c transition curve should be indirectly controlled. The C_l–x_{tr}/c transition curve can be controlled via the prescription of the design angle of attack α^* for a segment since it has a direct effect on the pressure gradient and consequently boundary layer response. As a result, the α^*–ϕ curves of an airfoil are the main tool used in PROFOIL to control the C_l–x_{tr}/c transition curve and eventual shape of the airfoil.

XFOIL is an airfoil analysis tool that utilizes the panel method coupled with an integral boundary-layer method. XFOIL has shown to be well suited for low Reynolds number airfoil flow predictions with the presence of laminar separation bubbles. At low Reynolds numbers, the laminar separation bubble is the leading culprit of performance degradation via form drag. As a result, it is critical that transition on the designed airfoils be predicted well. Transition is predicted in XFOIL through the use of a semi-empirical e^n method that leverages linear stability theory. The value of n refers to the linear stability theory amplification factor, where for low turbulence environments, experiments have shown transition to occur at an amplification
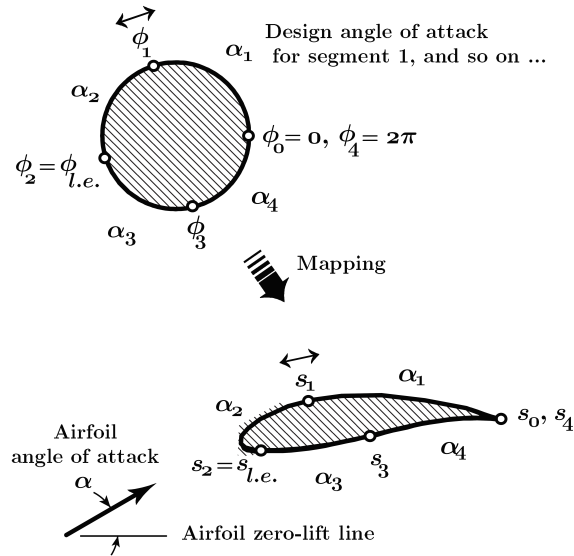
Figure 2. Parameterization of the circle as mapped to the airfoil.

factor of about 9 (n_{crit}). The n parameter in practical terms represents the background disturbance level and is critical in determining low Reynolds number airfoil performance. Linear stability theory derives from the application of the Orr-Somerfeld equations to the Falkner-Skan profile family.[17,18] For the current work, n_{crit} was set to the value of 9 (smooth wing, low turbulence environment) and each airfoil was divided into 240 panels. In the design, the arc limits around the airfoil were subdivided into 60 segments defined by ϕ.

III.   Application

A.   Design Requirements

A systematic approach was taken in the design of the bird-inspired airfoil families. Firstly, based on a literature review of typical bird profiles, maximum thicknesses of 4%, 5%, and 6% were chosen. To achieve a bird-like airfoil profile, a thin, feather-like aft region was maintained together with a low aft-loading requirement. As a result, the airfoil families were designed for the aerodynamic inviscid, quarter-chord, pitching moment coefficients (inviscid $C_{m,c/4}$) of -0.14, -0.20, and -0.26. These requirements allowed for the design of nine new airfoils that showed good C_l/C_d performance at Reynolds numbers between 60,000 to 150,000. The nine airfoils designed are tabulated in Table 1, and a profile view of the airfoils is shown in Fig. 3. The coordinates for each airfoil are provided in Appendix A.

Table 1. Airfoil Summary Table

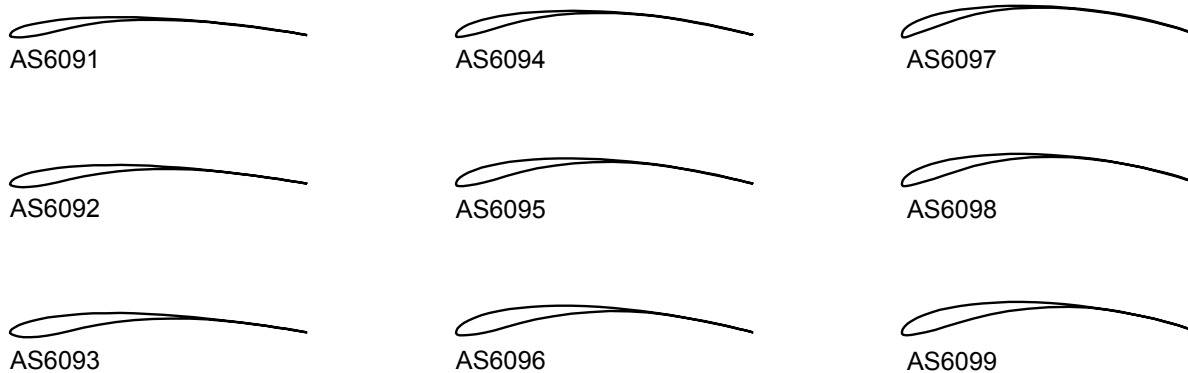| Airfoil	t/c	Inviscid $C_{m_{c/4}}$
AS6091	0.04	-0.14
AS6092	0.05	-0.14
AS6093	0.06	-0.14
AS6094	0.04	-0.20
AS6095	0.05	-0.20
AS6096	0.06	-0.20
AS6097	0.04	-0.26
AS6098	0.05	-0.26
AS6099	0.06	-0.26

Figure 3. All airfoil profiles.

B. Baseline Case

The baseline airfoil (AS6095), as shown in Fig. 4, was for an inviscid $C_{m,c/4}$ of −0.20 and maximum thickness of 5%. As per the design requirements, the PROFOIL airfoil segment velocity distributions were tailored to achieve a bulbous leading edge together with a thin, feather-like trailing edge. The α^*–ϕ curves for the upper and lower surface of the AS6095 airfoil are shown in Figs. 5(a,b). As previously described, the upper surface α^*–ϕ curve relates to the shape of the C_l–x_{tr} curve of the airfoil.[16] XFOIL predictions for the AS6091 airfoil at Reynolds numbers of 60,000, 100,000, and 150,000 are shown in Fig. 6. For all Reynolds numbers shown, the upper surface x_{tr} curve shows a gradual movement of the transition point toward the leading edge as C_l increases, closely following the shape of the α^*–ϕ curve [see Fig. 5(a)]. The lower surface α^*–ϕ curve [see Fig. 5(b)] was manipulated to achieve the desired airfoil shape.

The pressure distribution of the AS6095 at the best C_l/C_d condition at a Reynolds number of 100,000 is shown in Fig. 7. The bulbous leading edge of the AS6095 allows for a smooth pressure rise and gradual transition ramp. The best C_l/C_d lift coefficient (C_l) for the AS6095 is 1.35 which corresponds to an angle of attack of approximately 5 deg. The solid line in Fig. 7 represents the viscous pressure distribution, and the dashed line represents the inviscid pressure distribution. The viscous pressure distribution at a Reynolds number of 100,000 shows the existence of a small laminar separation bubble from the 45–65% chord on the upper surface. On the lower surface, the flow is fully attached and laminar. As can be observed in Fig. 6, no transition point exists on the lower surface at a C_l of 1.35 (maximum C_l/C_d). Smooth drag polars with a large drag buckets are observed especially at Reynolds numbers higher than 60,000. Finally, a sharp stall is observed in the airfoil accompanied by a rapid rise in drag.

The pressure distributions for the AS6095 at a Reynolds number of 100,000 over the low drag range (α = 0–7 deg) is shown in Fig. 8. The pressure distributions clearly show the movement of the upper surface laminar separation bubble toward the leading edge corresponding to the C_l–x_{tr} curve in Fig. 6. Similarly, the lower surface also shows the existence of a bubble that moves toward the leading edge with decreasing angle of attack.

Figure 4. AS9065 airfoil profile.
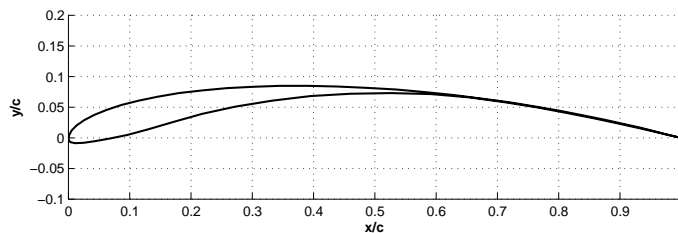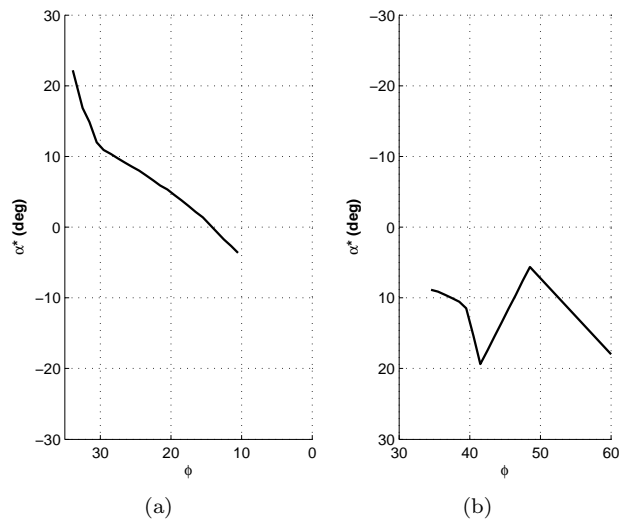
Figure 5. PROFOIL α^*–ϕ distributions for the AS6095 airfoil: (a) upper surface and (a) lower surface.
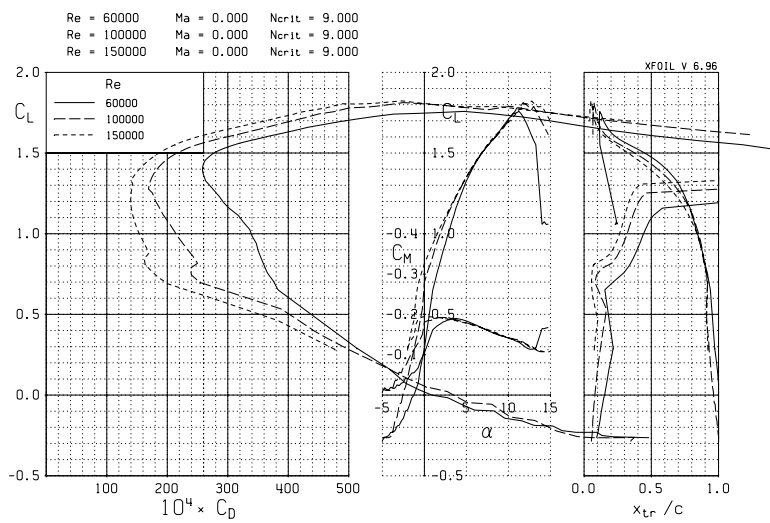

Figure 6. XFOIL predictions for the AS6095 airfoil at Reynolds numbers of 60,000, 100,000, and 150,000.
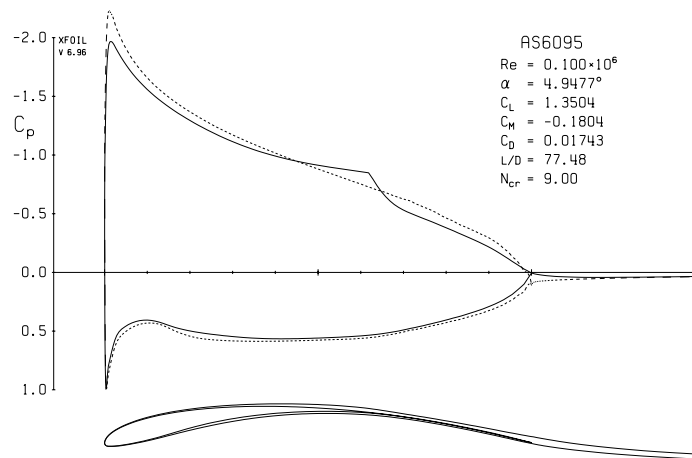
Figure 7. C_p distribution for the AS6095 airfoil at best C_l/C_d at a Reynolds numbers of 100,000.
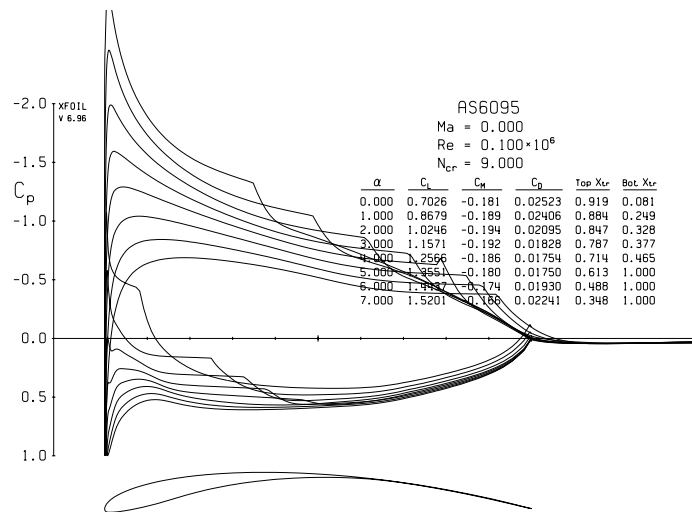
Figure 8. C_p distribution for the AS6095 airfoil at $\alpha = 0$ to 7 deg at a Reynolds numbers of 100,000.

C.   Baseline Airfoil Family

Designed to the same inviscid $C_{m,c/4}$ of -0.20, the AS6094 (4%) and AS6096 (6%) airfoils are coplotted with the AS6095 airfoil in Fig. 9. In addition, the PROFOIL upper and lower surface α^*–ϕ curves for the airfoil family are shown in Fig. 10. The α^*–ϕ curves for both the upper and lower surfaces of the airfoils shows a systematic trend in the α^*–ϕ prescriptions for each airfoil. For the upper surface, as the thickness increases, a steeper α^*–ϕ curve is prescribed. These prescriptions correspond well to the XFOIL predictions for the three airfoils (Figs. 6, 12, and 13), where the C_l–x_{tr} curves are observed to be steeper with increasing thickness.

The pressure distributions of the AS6094 and AS6096 airfoils at their respective maximum C_l/C_d conditions are shown in Fig. 11(a,b). Similar to the AS6095 airfoil, a separation bubble exists around the 45–65% chord region on the upper surface of the airfoil. The size of the separation bubble grows with thickness thereby reducing the maximum C_l/C_d possible. The flow is also attached along the lower surface of the air-
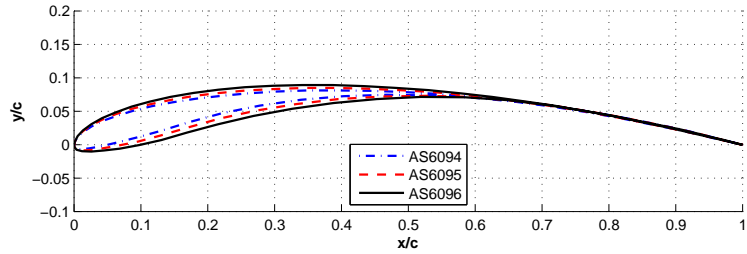
Figure 9. Coplot of the baseline family (inviscid $C_{m,c/4}=-0.20$) of bird-like airfoils (AS6094, AS6095, and AS6096).
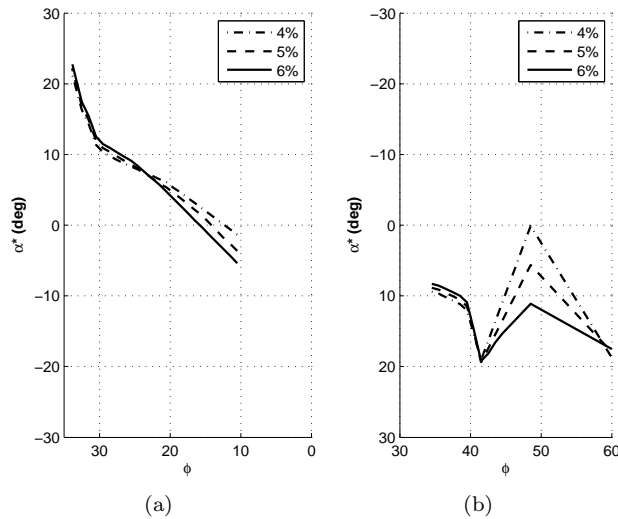
Figure 10. PROFOIL $\alpha^*-\phi$ distributions for $C_{m,c/4}=-0.20$ airfoils: (a) upper surface and (a) lower surface.

Figure 11. C_p distributions for $C_{m,c/4}=-0.20$ airfoils at best C_l/C_d for a Reynolds number of 100,000: (a) AS6094 (4%) and (b) AS6096 (6%).

foil. Interestingly, the lift coefficients corresponding to the best C_l/C_d for all three airfoils are approximately 1.35 and the viscous $C_{m,c/4}$ for the airfoils are approximately -0.18 (compared to designed inviscid $C_{m,c/4}$ of -0.20). The main difference observed in the airfoils is in the C_d values as per the polars shown in Figs. 6, 12 and 13. There is an increase in the size of the drag bucket for the thicker AS6096 airfoil. All airfoils in this family, however, still stall sharply with the thickest airfoil (AS6096) stalling at the lowest angle of attack among the airfoil family.

Figure 12. XFOIL predictions for the AS6094 airfoil at Reynolds numbers of 60,000, 100,000, and 150,000.

Figure 13. XFOIL predictions for the AS6096 airfoil at Reynolds numbers of 60,000, 100,000, and 150,000.

D. Lower Moment Airfoil Family

Similar to the baseline (inviscid $C_{m,c/4}=-0.20$) airfoil family, another family of airfoils was designed to have an inviscid $C_{m,c/4}$ of -0.14. The AS6091 (4%), AS6092 (5%), and AS6093 (6%) airfoils are coplotted in Fig. 14. Correspondingly, the PROFOIL α^*–ϕ distributions on the upper and lower surfaces for the $C_{m,c/4}=-0.14$ family airfoils are shown in Figs. 15(a,b). Again, the α^*–ϕ curves were varied systematically. As a result, the upper surface α^*–ϕ distributions become increasingly convex and steeper with increasing thickness. The enforced distributions generate airfoils whose upper surface C_l–x_{tr} movement becomes steeper with increasing thickness as shown in Figs. 17, 18, and 19.

Finally, unlike the baseline airfoil family, the pressure distributions at maximum C_l/C_d for the lower moment family airfoils [see Fig. 16(a–c)] show a less clear-cut difference in the separation bubble size. As a result, at roughly the same C_l, a small difference in C_l/C_d is observed between the AS6091, AS6092, and AS6093 airfoils. Best C_l/C_d performance for the three airfoil occurs at an approximate C_l of 1.05 and viscous $C_{m,c/4}$ of -0.125. A smaller variation in the size of the low drag bucket is observed for the three airfoils. Stall again is abrupt for all airfoils in this lower moment family.
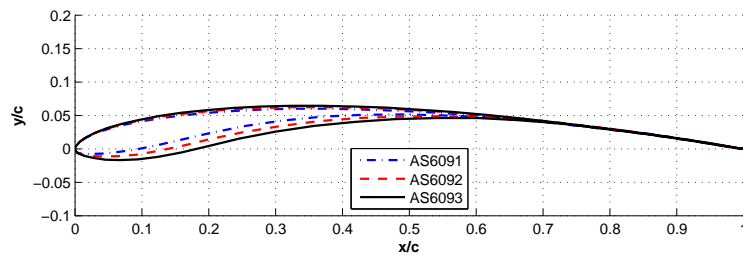

Figure 14. Coplot of the lower-moment family (inviscid $C_{m,c/4}=-0.14$) of bird-like airfoils (AS6091, AS6092, and AS6093).
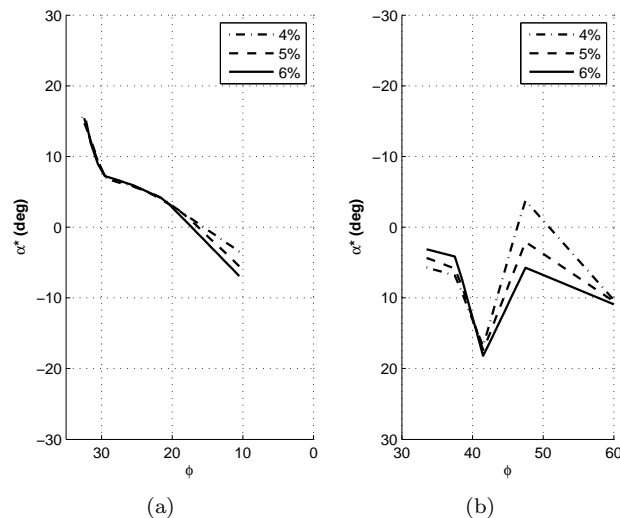
Figure 15. PROFOIL α^*–ϕ distributions for $C_{m,c/4}=-0.14$ airfoils: (a) upper surface and (a) lower surface.
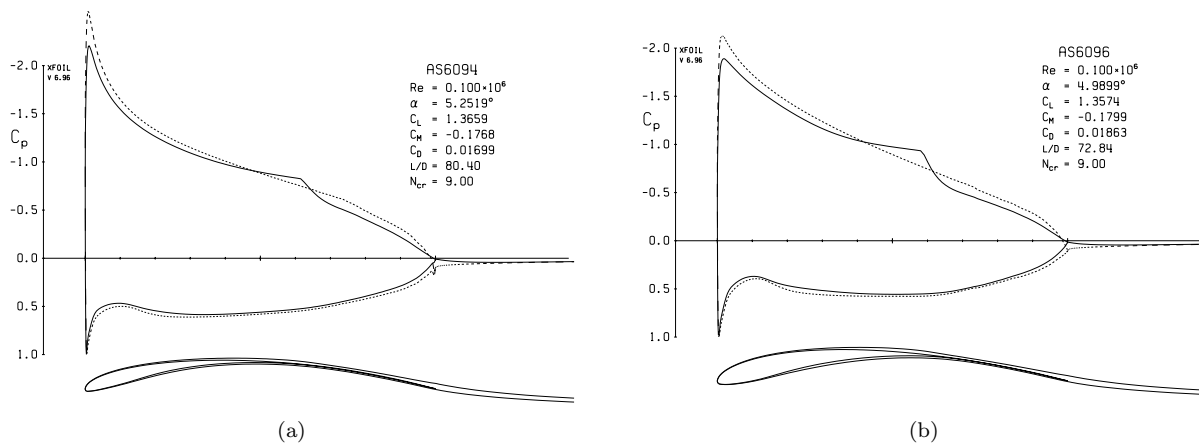
(a)

(b)

(c)
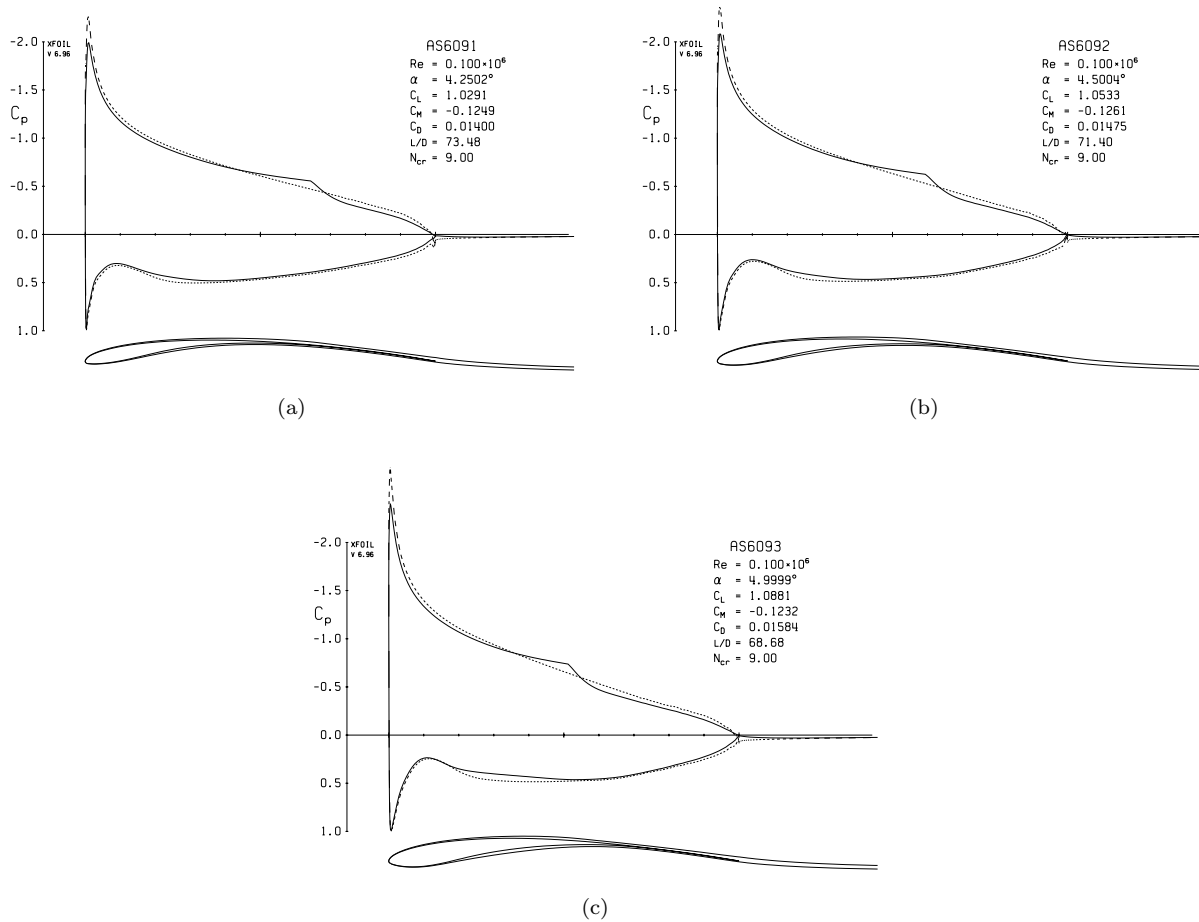
Figure 16. C_p distributions for $C_{m,c/4}=-0.14$ airfoils at best C_l/C_d for a Reynolds number of 100,000: (a) AS6091 (4%), (b) AS6092 (5%), and (c) AS6093 (6%).
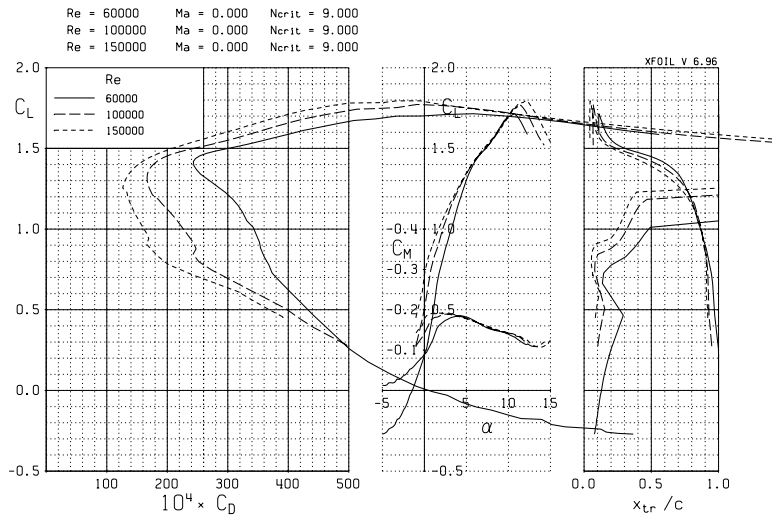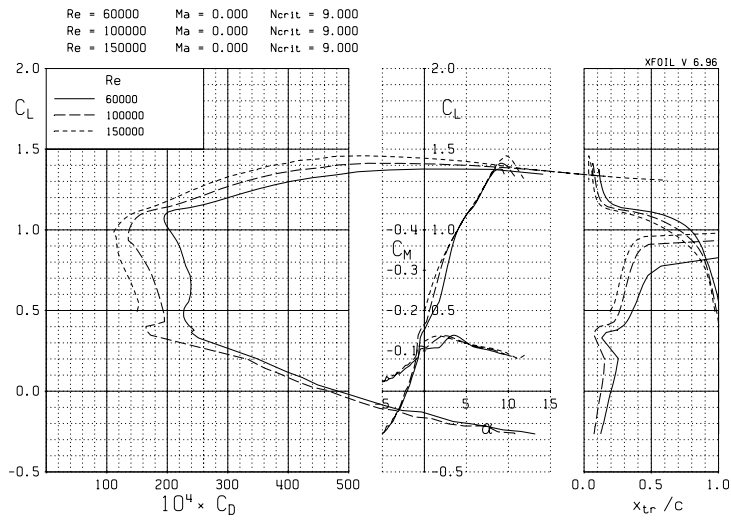
Figure 17. XFOIL predictions for the AS6091 airfoil at Reynolds numbers of 60,000, 100,000, and 150,000.
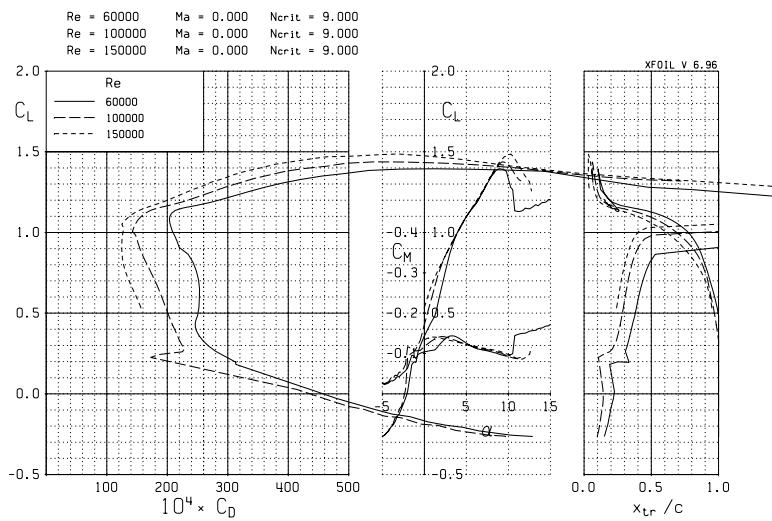
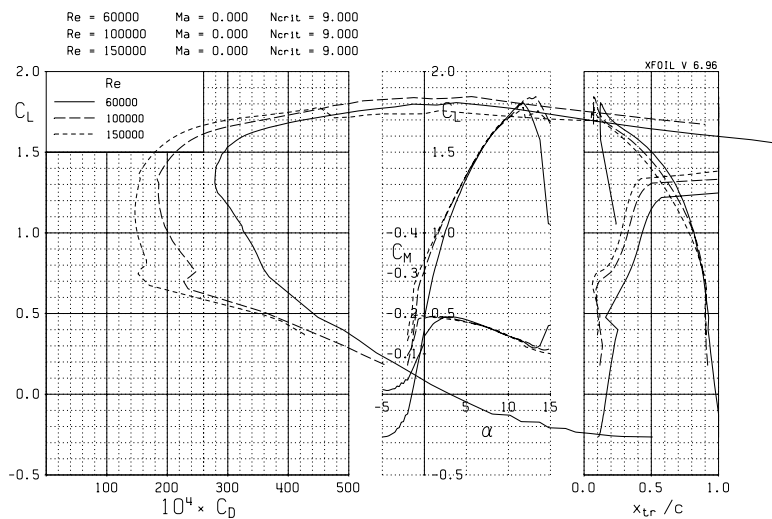**Figure 18. XFOIL predictions for the AS6092 airfoil at Reynolds numbers of 60,000, 100,000, and 150,000.**
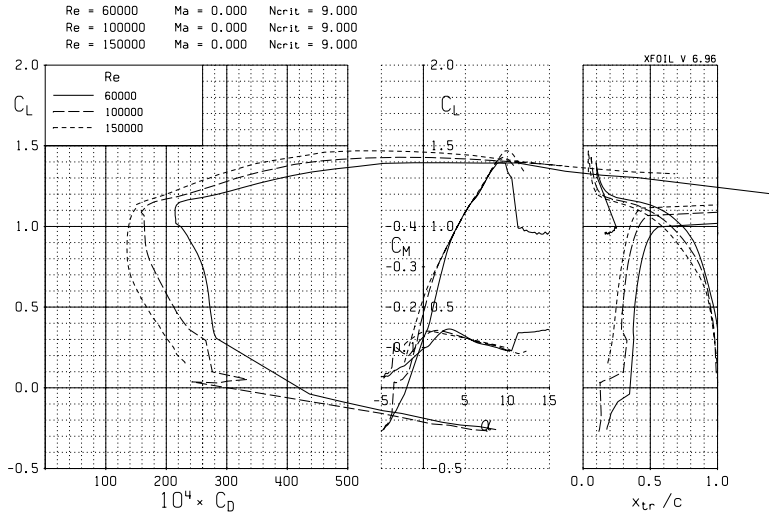
Figure 19. XFOIL predictions for the AS6093 airfoil at Reynolds numbers of 60,000, 100,000, and 150,000.

E. Higher Moment Airfoil Family

The final family of airfoils are the higher moment airfoil family (inviscid $C_{m,c/4}=-0.26$). The AS6097, AS6098, and AS6099 airfoils that make this higher moment airfoil family are coplotted in Fig. 20 showing its highly cambered and bulbous leading edge profile. The PROFOIL $\alpha^*-\phi$ upper and lower surface curves used to generate the airfoil family geometries are presented in Figs. 21(a,b) respectively. Similar to the baseline and lower moment families, the upper surface $\alpha^*-\phi$ curve becomes progressively steeper with increasing thickness of the airfoil.

The pressure distributions for the three airfoils (AS6097, AS6098, and AS6099) at their respective maximum C_l/C_d are shown in Figs. 22(a–c). The maximum C_l/C_d for each airfoil occurs at a C_l of approximately 1.6 and viscous $C_{m,c/4}$ of approximately -0.023. The largest C_l/C_d occurs for thinner airfoils that also have smaller laminar separation bubbles. Finally, Figs. 23, 24, and 25 show a widening of the drag bucket and correspondingly a steeper upper surface transition point shift with increasing thickness as prescribed by the upper surface $\alpha^*-\phi$ curves. For the lower surface, the transition point shifts toward the leading edge with decreasing angle of attack.
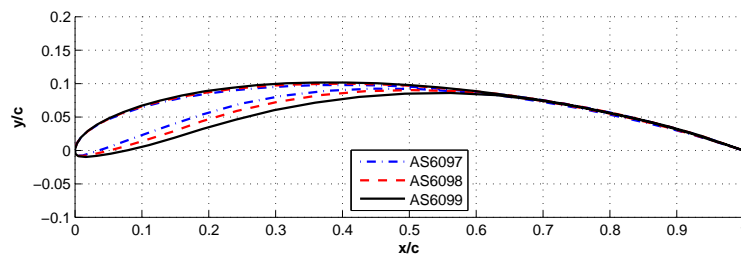
Figure 20. Coplot of the higher-moment family (inviscid $C_{m,c/4}=-0.26$) of bird-like airfoils (AS6091, AS6092, and AS6093).

Figure 21. PROFOIL α^*–ϕ distributions for $C_{m,c/4}=-0.26$ airfoils: (a) upper surface and (a) lower surface.
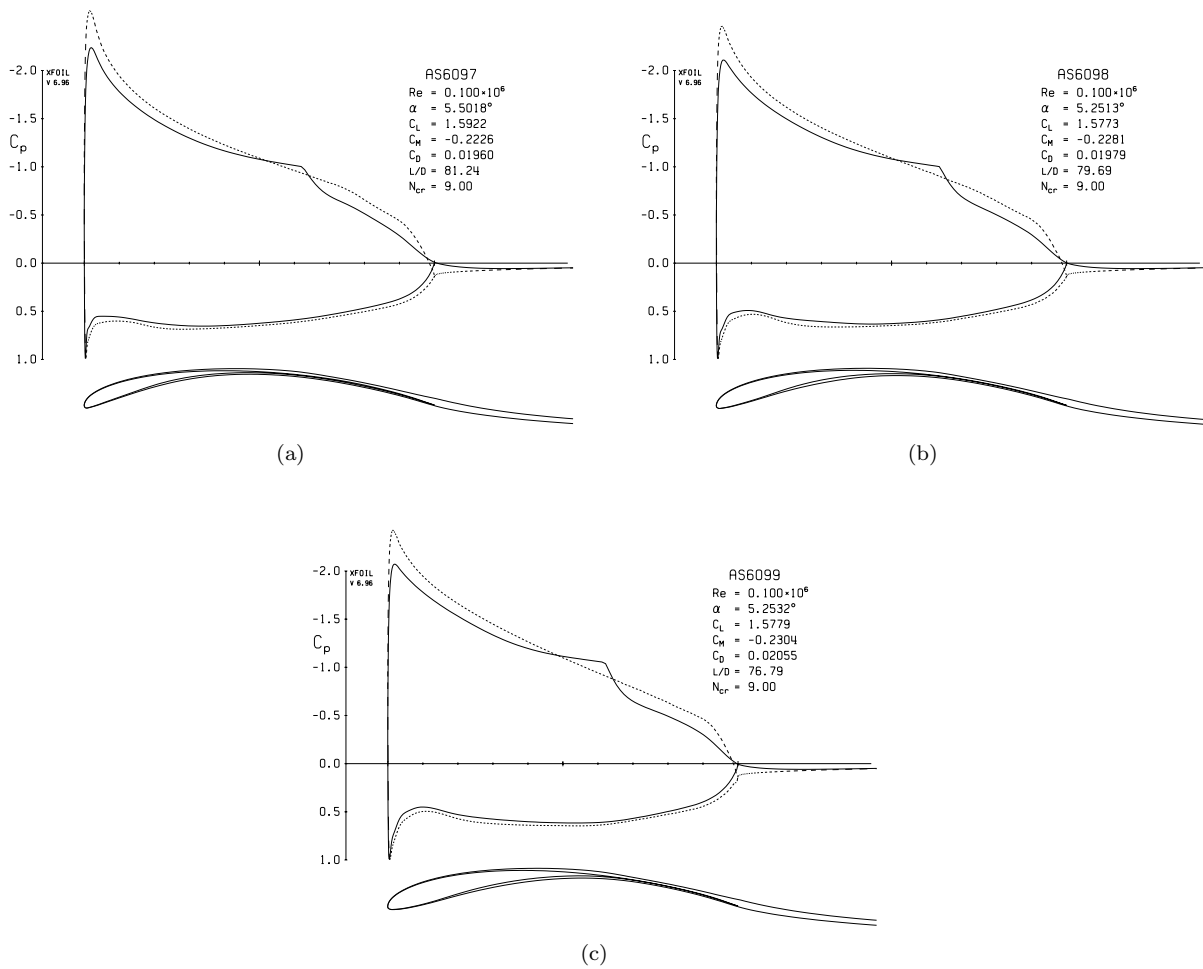
Figure 22. C_p distributions for $C_{m,c/4}=-0.14$ airfoils at best C_l/C_d for a Reynolds number of 100,000: (a) AS6097 (4%), (b) AS6098 (5%), and (c) AS6099 (6%).
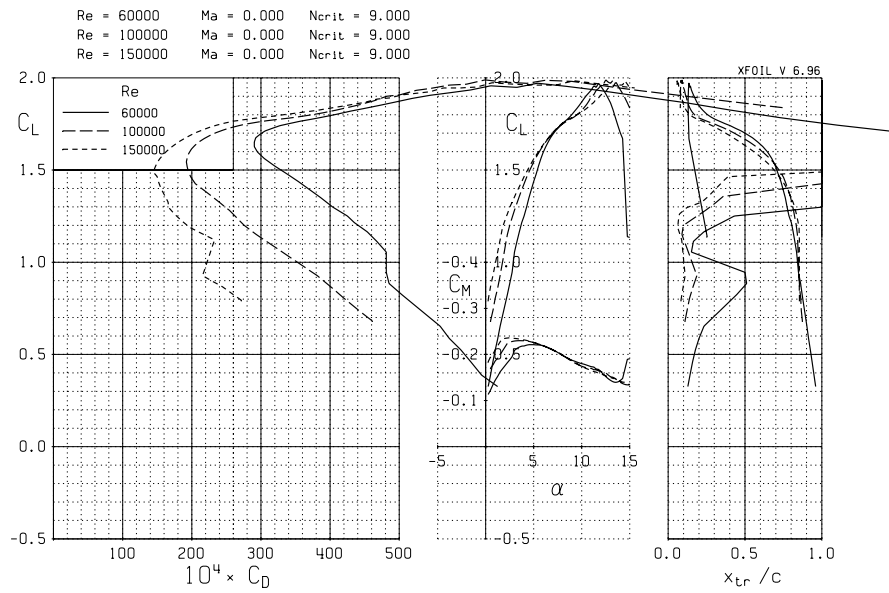
Figure 23. XFOIL predictions for the AS6097 airfoil at Reynolds numbers of 60,000, 100,000, and 150,000.
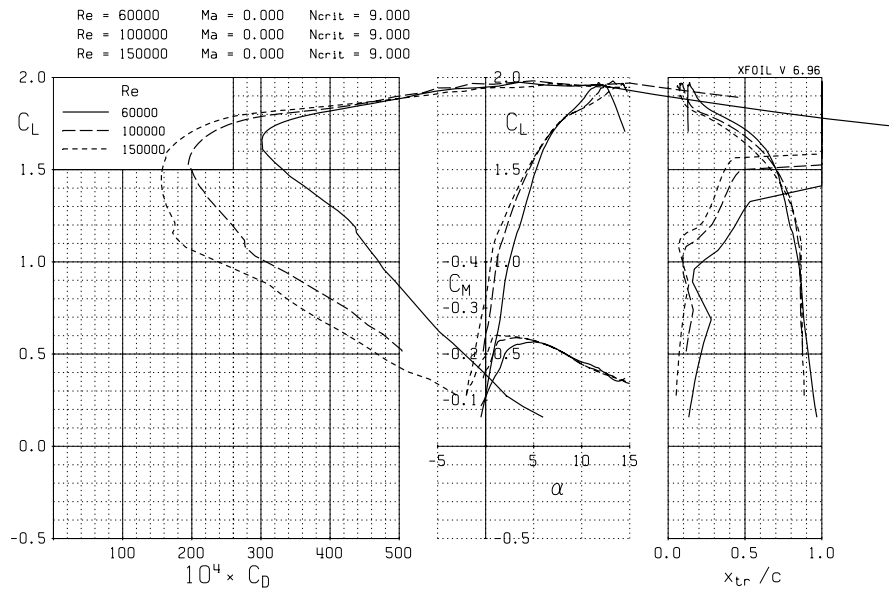
Figure 24. XFOIL predictions for the AS6098 airfoil at Reynolds numbers of 60,000, 100,000, and 150,000.
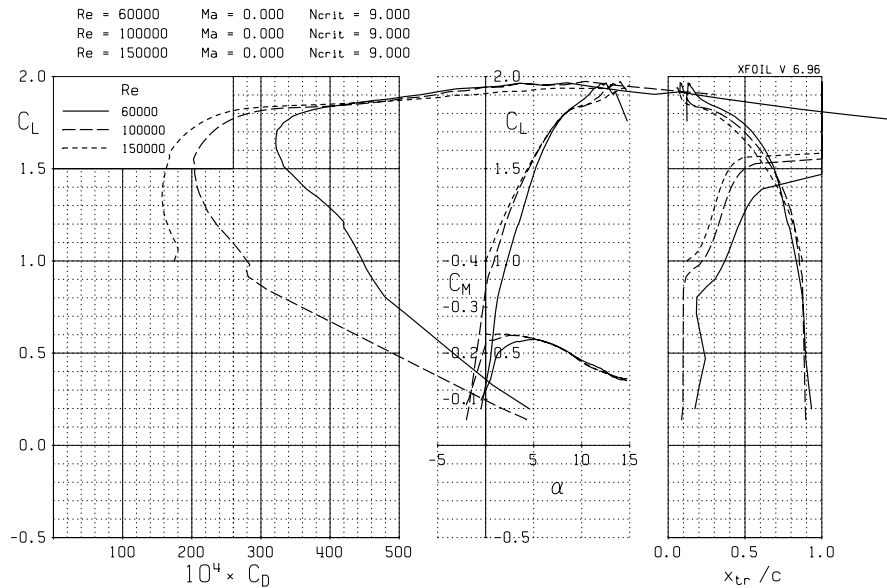
Figure 25. XFOIL predictions for the AS6099 airfoil at Reynolds numbers of 60,000, 100,000, and 150,000.

F.   Summary

The nine airfoils presented in this paper were designed to have bird-like profiles. Three different airfoil families were created based on the inviscid moments (inviscid $C_{m,c/4}$) of -0.14, -0.20, and -0.26. To better understand the differences between the three airfoil families, coplots of all airfoil polars are shown in Figs. 26, 27, and 28 for the Reynolds numbers of 60,000, 100,000 and 150,000 respectively. From Figs. 26–28, the general trends observed for this family of airfoils are the following:

- For a constant $C_{m,c/4}$, as t/c decreases, $C_{d_{min}}$ decreases.

- For a constant $C_{m,c/4}$, as t/c decreases, the low drag bucket range narrows.

- Drag bucket narrows with increase in $C_{m,c/4}$ from -0.14 to -0.26.

- Drag bucket widens with increase in Reynolds number.

- Lift coefficient corresponding to $C_{d_{min}}$ increases with $C_{m,c/4}$.

- $C_{d_{min}}$ increases with increase in $C_{m,c/4}$.

A summary of the performance of all airfoils at the best C_l/C_d condition at a Reynolds number of 100,000 is presented in Table 2. Note that with slight modification of the PROFOIL input design parameters, the airfoils can be designed to have a finite trailing edge thickness together with a thicker aft region for manufacturing ease. Moreover, the leading edge and nearby region can also be altered by changes in the α^*–ϕ distribution.

Table 2. Airfoil Performance at Best C_l/C_d ($Re =$100,000)

Airfoil	t/c	camber	$(C_l/C_d)_{max}$	α (deg)	C_l	viscous $C_{m_{c/4}}$
AS6091	0.04	0.055	73.48	4.25	1.03	−0.125
AS6092	0.05	0.054	71.40	4.50	1.05	−0.126
AS6093	0.06	0.053	68.68	5.00	1.09	−0.123
AS6094	0.04	0.078	80.40	5.25	1.37	−0.177
AS6095	0.05	0.078	77.48	4.95	1.35	−0.180
AS6096	0.06	0.078	72.84	4.99	1.36	−0.180
AS6097	0.04	0.095	81.24	5.50	1.59	−0.22
AS6098	0.05	0.095	79.69	5.25	1.58	−0.23
AS6099	0.06	0.092	76.79	5.25	1.58	−0.23
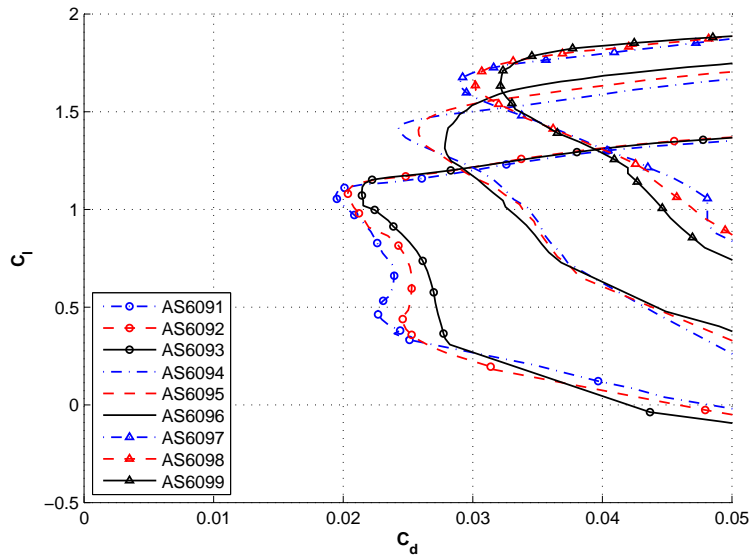
Figure 26. Drag polars for all airfoils at a Reynolds numbers of 60,000.
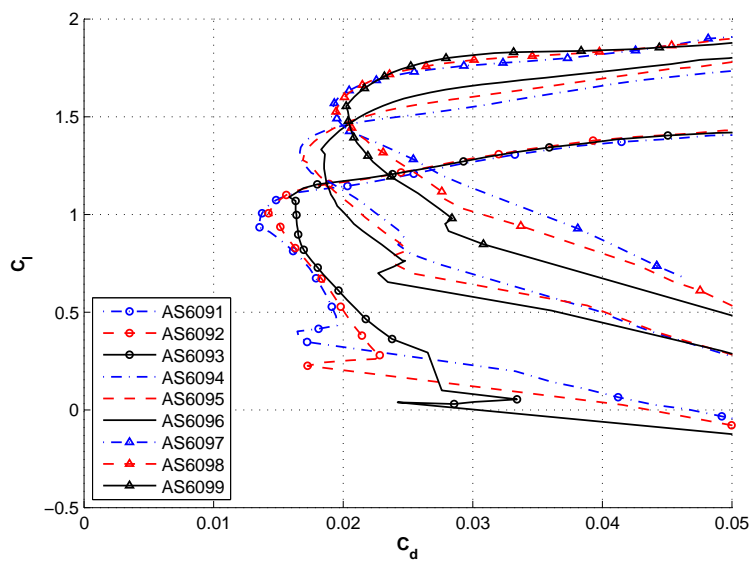
Figure 27. Drag polars for all airfoils at a Reynolds numbers of 100,000.
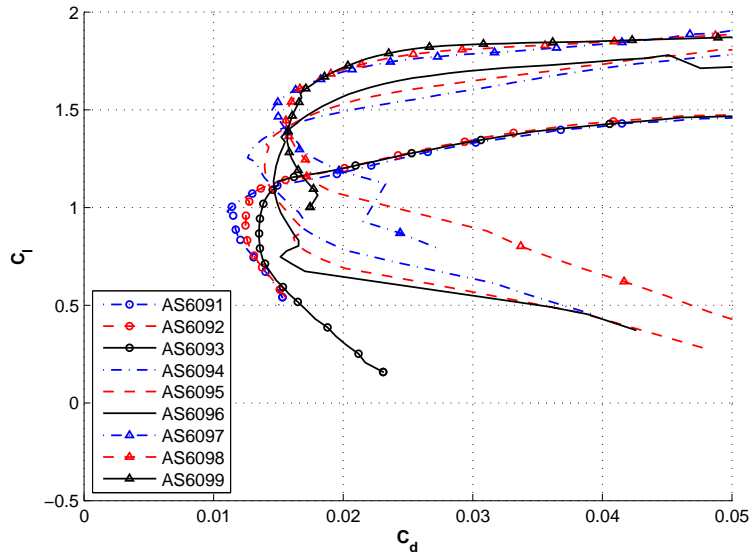
Figure 28. Drag polars for all airfoils at a Reynolds numbers of 150,000.

IV.   Conclusions

The rapidly growing field of bio-inspired micro vehicle design in recent years has demanded the need to better understand and mimic avian flight characteristics especially at low Reynolds numbers. The approach taken in this paper was to design three bird-like airfoil families of increasing inviscid, quarter-chord moments $C_{m,c/4}$ of -0.14 to -0.26. A total of nine new airfoils were designed with maximum thicknesses of 4–6%.

Designed using multipoint inverse design methods, all airfoils geometrically were characterized by a bulbous leading edge followed by a thin, feather-like aft region. The upper surface of the airfoil was designed to promote smooth transition from laminar-to-turbulent flow and a small laminar separation bubble. The lower surface was more actively manipulated to acheive the desired bird-like profile shape. In terms of performance, all airfoils showed well-defined drag buckets, high C_l/C_d performance, predictable transition characteristics, and high best C_l/C_d lift coefficients to allow for its use in MAVs requiring high wing loadings.

References

[1]Lilienthal, O., *Birdflight As the Basis of Aviation: A Contribution Towards a System of Aviation*, Markowski International Publishers, Hummestown, PA, 1st ed., 2000.

[2]McMasters, J. H., "The Biomechanics of Flight: Many Possible Solutions Looking for Problems," *International Journal of Engineering Education*, Vol. 20, No. 3, 2004, pp. 398–404.

[3]Raney, D. and Waszak, M., "Biologically Inspired Micro-Flight Research," SAE Technical Paper 2003-01-3042, Montreal, Quebec, Canada, September 2003.

[4]McMasters, J. H. and Henderson, M. L., "Low-Speed Single-Element Airfoil Synthesis," *Technical Soaring*, Vol. 6, No. 2, 1980, pp. 1–21.

[5]Altshuler, D. L., Bachlman, J. W., Dakin, R., Gaede, A. H., Goller, B., Lentink, D., Segre, P. S., and Skandalis, D. A., "The Biophysics of Bird Flight: Functional Relationships Integrate Aerodynamics, Morphology, Kinematics, Muscles, and Sensors," *Canandian Journal of Zoology*, Vol. 93, 2015, pp. 961–975.

[6]Lentink, D., Miller, U. K., Stamhuis, E. J., de Kat, R., van Gestel, W., Veldhius, L. L. M., Henningsson, P., Hedenstrőm, A., Videler, J. J., and van Leeuwen, J. L., "How Swifts Control their Glide Performance with Morphing Wings," *Nature*, Vol. 446, 2007, pp. 1082–1085.

[7]Altshuler, D. L., Dudley, R., and Ellington, C. P., "Aerodynamic Forces of Revolving Hummingbird Wings and Wing Models," *Journal of Zoology (London)*, Vol. 264, 2004, pp. 327–332.

[8]Nachtigall, W. and Wieser, J., "Profilmessungen am Taubenflűgel," *Zeitschrift fur vergleichende Physiologies*, Vol. 52, 1966, pp. 333–346.

[9]Oehme, H. and Kitzler, U., "On the Geometry of the Avian Wing," Studies on the Biophysics and Physiology of Avian Flight II, NASA TT-F-16901, Feb. 1975.

[10]Withers, P. C., "An Aerodynamic Analysis of Bird Wings and Fixed Aerofoils," *Journal of Experimental Biology*, Vol. 90, 1981, pp. 143–162.

[11]Liu, T., Kuykendoll, K., Rhew, R., and Jones, S., "Avian Wing Geometry and Kinematics," *AIAA Journal*, Vol. 44, No. 5, 2006, pp. 954–963.

[12]Klän, S., Bachmann, T., Klaas, M., Wagner, H., and Schröder, W., "Experimental Analysis of the Flow Field over a Novel Owl Based Airfoil," *Experiments in Fluids*, Vol. 46, No. 5, 2009, pp. 975–989.

[13]Selig, M. S. and Maughmer, M. D., "Multipoint Inverse Airfoil Design Method Based on Conformal Mapping," *AIAA Journal*, Vol. 30, No. 5, May 1992, pp. 1162–1170.

[14]Selig, M. S. and Maughmer, M. D., "Generalized Multipoint Inverse Airfoil Design," *AIAA Journal*, Vol. 30, No. 11, November 1992, pp. 2618–2625.

[15]Selig, M. S., *Multi-Point Inverse Design of Isolated Airfoils and Airfoils in Cascade in Incompressible Flow*, PhD dissertation, Dept. of Aerospace Engineering, Pennsylvania State Univ., University Park, PA, May 1992.

[16]Selig, M. S., "Low Reynolds Number Airfoil Design," VKI Lecture Series – Low Reynolds Number Aerodynamics on Aircraft Including Applications in Emerging UAV Technology, von Karman Institute for Fluid Dynamics (VKI) Lecture Series, RTO/AVT-VKI-104, Sint-Genesius-Rode, Belgium, Nov. 2003.

[17]Drela, M., "Viscous-Inviscid Analysis of Transonic and Low Reynolds Number Airfoils," *AIAA Journal*, Vol. 25, No. 10, 1987, pp. 1347–1355.

[18]Drela, M., "XFOIL: An Analysis and Design System for Low Reynolds Number Airfoils," *Low Reynolds Number Aerodynamics*, edited by T. J. Mueller, Vol. 54 of *Lecture Notes in Engineering*, Springer-Verlag, New York, June 1988, pp. 1–12.

A Tabulated Airfoil Coordinates

AS6091

$C_{m,c/4} = -0.14$, 4%

x/c	y/c
0.997162	0.000460
0.988765	0.001881
0.975083	0.004261
0.956444	0.007492
0.933179	0.011391
0.905574	0.015728
0.873865	0.020341
0.838354	0.025159
0.799464	0.030117
0.757659	0.035087
0.713414	0.039929
0.667185	0.044490
0.619448	0.048666
0.570692	0.052336
0.521411	0.055408
0.472093	0.057779
0.423219	0.059383
0.375257	0.060147
0.328654	0.060037
0.283837	0.059021
0.241198	0.057101
0.201107	0.054301
0.163910	0.050698
0.129939	0.046360
0.099481	0.041383
0.072799	0.035865
0.050097	0.029942
0.031576	0.023763
0.017387	0.017462
0.007613	0.011061
0.002001	0.004628
0.000144	-0.001232
0.002471	-0.005123
0.009906	-0.007051
0.022652	-0.007752
0.040398	-0.007126
0.062900	-0.005027
0.090065	-0.001009
0.122188	0.005344
0.159912	0.014005
0.204052	0.024407
0.254882	0.034611
0.311093	0.042714
0.370683	0.048214
0.432068	0.051093
0.493877	0.051607
0.554949	0.050101
0.614383	0.047071
0.671397	0.042764
0.725166	0.037563
0.775091	0.031972
0.820785	0.026347
0.861906	0.020908
0.898150	0.015811
0.929167	0.011152
0.954663	0.007144
0.974503	0.003967
0.988664	0.001728
0.997163	0.000424
1.000000	-0.000000

AS6092

$C_{m,c/4} = -0.14$, 5%

x/c	y/c
0.997145	0.000459
0.988697	0.001873
0.974921	0.004238
0.956135	0.007450
0.932664	0.011340
0.904799	0.015701
0.872795	0.020378
0.836970	0.025300
0.797750	0.030401
0.755605	0.035568
0.711039	0.040684
0.664570	0.045583
0.616691	0.050103
0.567882	0.054094
0.518626	0.057438
0.469395	0.060019
0.420649	0.061758
0.372839	0.062588
0.326395	0.062478
0.281737	0.061416
0.239271	0.059419
0.199377	0.056512
0.162401	0.052743
0.128658	0.048177
0.098423	0.042917
0.071947	0.037080
0.049436	0.030800
0.031067	0.024238
0.016987	0.017570
0.007292	0.010886
0.001838	0.004285
0.000257	-0.001591
0.003415	-0.005813
0.011902	-0.008722
0.025199	-0.010735
0.043118	-0.011546
0.065421	-0.010921
0.091998	-0.008356
0.123090	-0.003336
0.159303	0.004316
0.201545	0.014294
0.250382	0.024870
0.304876	0.034098
0.363283	0.041246
0.424117	0.046062
0.486037	0.048558
0.547846	0.048869
0.608565	0.047249
0.667099	0.043651
0.722180	0.038536
0.773071	0.032799
0.819449	0.026934
0.861028	0.021254
0.897560	0.015965
0.928758	0.011195
0.954383	0.007141
0.974330	0.003959
0.988579	0.001725
0.997140	0.000425
1.000000	0.000000

AS6093

$C_{m,c/4} = -0.14$, 6%

x/c	y/c
0.997127	0.000458
0.988625	0.001866
0.974759	0.004217
0.955842	0.007407
0.932194	0.011270
0.904106	0.015608
0.871836	0.020269
0.835704	0.025194
0.796133	0.030320
0.753590	0.035563
0.708615	0.040848
0.661794	0.046013
0.613651	0.050833
0.564669	0.055138
0.515328	0.058781
0.466101	0.061641
0.417446	0.063608
0.369805	0.064596
0.323596	0.064553
0.279209	0.063453
0.237009	0.061311
0.197351	0.058191
0.160586	0.054176
0.127037	0.049345
0.096989	0.043793
0.070685	0.037651
0.048335	0.031067
0.030116	0.024214
0.016188	0.017289
0.006660	0.010424
0.001480	0.003749
0.000416	-0.001971
0.004467	-0.006475
0.013920	-0.010400
0.027838	-0.013690
0.046015	-0.015956
0.068164	-0.016854
0.094138	-0.015744
0.124196	-0.011961
0.158972	-0.005163
0.199523	0.004563
0.246706	0.015555
0.299830	0.025741
0.357284	0.034223
0.417636	0.040589
0.479563	0.044685
0.541845	0.046500
0.603460	0.046117
0.663100	0.043268
0.719186	0.038449
0.770867	0.032817
0.817855	0.026957
0.859895	0.021249
0.896766	0.015927
0.928216	0.011146
0.954032	0.007096
0.974126	0.003931
0.988484	0.001713
0.997116	0.000423
1.000000	0.000000

AS6094

$C_{m,c/4} = -0.20$, 4%

x/c	y/c
0.997150	0.000662
0.988752	0.002715
0.975165	0.006171
0.956812	0.010872
0.934082	0.016541
0.907276	0.022850
0.876602	0.029550
0.842362	0.036543
0.805011	0.043675
0.765041	0.050710
0.722819	0.057257
0.678575	0.063131
0.632673	0.068333
0.585582	0.072785
0.537768	0.076387
0.489692	0.079068
0.441812	0.080750
0.394574	0.081394
0.348413	0.080962
0.303741	0.079457
0.260957	0.076895

x/c	y/c
0.220442	0.073331
0.182565	0.068819
0.147649	0.063444
0.115997	0.057293
0.087858	0.050479
0.063455	0.043132
0.042941	0.035405
0.026455	0.027476
0.014057	0.019523
0.005758	0.011683
0.001275	0.004218
0.000371	-0.002249
0.002821	-0.006226
0.009992	-0.007101
0.023140	-0.005595
0.041873	-0.002009
0.066159	0.003604
0.095872	0.011211
0.131095	0.021225
0.172895	0.033851
0.222366	0.047101
0.278564	0.058455
0.339421	0.066964
0.403170	0.072343
0.468278	0.074594
0.533369	0.073911
0.597257	0.070519
0.658593	0.064577
0.716021	0.056786
0.768818	0.048256
0.816694	0.039596
0.859427	0.031257
0.896815	0.023467
0.928568	0.016424
0.954447	0.010423
0.974439	0.005743
0.988639	0.002482
0.997154	0.000610
1.000000	-0.000000

AS6095

$C_{m,c/4} = -0.20$, 5%

x/c	y/c
0.997136	0.000665
0.988696	0.002720
0.975031	0.006161
0.956545	0.010836
0.933616	0.016481
0.906545	0.022788
0.875554	0.029520
0.840951	0.036580
0.803186	0.043823
0.762749	0.051036
0.720050	0.057890
0.675406	0.064186
0.629212	0.069849
0.581927	0.074764
0.534004	0.078811
0.485893	0.081907
0.438051	0.083971
0.390925	0.084952
0.344948	0.084803
0.300529	0.083514
0.258067	0.081091
0.217932	0.077567
0.180471	0.072974
0.145979	0.067391
0.114727	0.060920
0.086947	0.053697
0.062848	0.045864
0.042572	0.037597
0.026252	0.029106
0.013957	0.020598
0.005718	0.012238
0.001294	0.004313
0.000465	-0.002553
0.003348	-0.006876
0.011152	-0.008389
0.024671	-0.007931
0.043499	-0.005582
0.067522	-0.001315
0.096548	0.004967
0.130617	0.013834
0.170813	0.025751
0.218433	0.038999
0.272913	0.051123
0.332489	0.061006
0.395557	0.068128
0.460647	0.072252
0.526379	0.073335
0.591531	0.071348
0.654423	0.066059
0.713187	0.058251
0.766942	0.049469
0.815484	0.040484
0.858652	0.031830
0.896307	0.023790
0.928223	0.016587
0.954219	0.010500
0.974304	0.005778
0.988577	0.002498
0.997138	0.000614
1.000000	-0.000000

AS6096

$C_{m,c/4} = -0.20$, 6%

x/c	y/c
0.997119	0.000674
0.988633	0.002749
0.974893	0.006211
0.956295	0.010899
0.933207	0.016549
0.905922	0.022858
0.874653	0.029596
0.839702	0.036678
0.801509	0.043979
0.760557	0.051323
0.717302	0.058460
0.672162	0.065190
0.625578	0.071364
0.578015	0.076836
0.529938	0.081455
0.481804	0.085104
0.434062	0.087673
0.387146	0.089081
0.341474	0.089254
0.297436	0.088169
0.255403	0.085813
0.215713	0.082219
0.178688	0.077441
0.144611	0.071564
0.113736	0.064694
0.086270	0.056984
0.062409	0.048617
0.042307	0.039792
0.026099	0.030738
0.013871	0.021685
0.005668	0.012820
0.001287	0.004444
0.000530	-0.002812
0.003765	-0.007526
0.012086	-0.009669
0.025932	-0.010128
0.044889	-0.008847
0.068787	-0.005742
0.097399	-0.000636
0.130723	0.007100
0.169753	0.018035
0.215782	0.030792
0.268546	0.043144
0.326611	0.053902
0.388582	0.062437
0.453168	0.068328
0.519092	0.071276
0.585175	0.070951
0.649449	0.066635
0.709509	0.059116
0.764270	0.050344
0.813587	0.041241
0.857338	0.032419
0.895423	0.024211
0.927651	0.016864
0.953871	0.010668
0.974117	0.005869
0.988497	0.002537
0.997119	0.000623
1.000000	0.000000

AS6097

$C_{m,c/4} = -0.26$, 4%

x/c	y/c
0.997161	0.000892
0.988867	0.003647
0.975604	0.008229
0.957894	0.014351
0.936145	0.021568
0.910583	0.029385
0.881276	0.037487
0.848431	0.045792
0.812477	0.054167
0.773882	0.062346
0.732978	0.069940
0.689963	0.076738
0.645177	0.082757
0.599067	0.087893
0.552074	0.092063
0.504641	0.095185
0.457218	0.097210
0.410257	0.098085
0.364197	0.097792
0.319466	0.096308
0.276470	0.093652
0.235591	0.089834
0.197171	0.084911
0.161534	0.078968
0.128966	0.072103
0.099722	0.064429
0.074005	0.056105
0.052002	0.047310
0.033867	0.038255
0.019753	0.029069
0.009594	0.019827
0.003169	0.010852
0.000191	0.002630
0.000444	-0.004136
0.003715	-0.007782
0.011501	-0.007355
0.025427	-0.003427
0.045583	0.003471
0.072182	0.013011
0.105256	0.024744
0.144899	0.038677

x/c	y/c
0.192109	0.054570
0.247699	0.069818
0.310021	0.081587
0.376335	0.089093
0.444474	0.092373
0.512679	0.091764
0.579471	0.087789
0.643496	0.080946
0.703562	0.072090
0.758961	0.062177
0.809309	0.051877
0.854311	0.041646
0.893685	0.031761
0.926961	0.022476
0.953798	0.014360
0.974263	0.007926
0.988624	0.003423
0.997160	0.000835
1.000000	-0.000000

AS6098

$C_{m,c/4} = -0.26$, 5%

x/c	y/c
0.997158	0.000913
0.988865	0.003722
0.975624	0.008371
0.957954	0.014546
0.936248	0.021780
0.910710	0.029565
0.881375	0.037586
0.848421	0.045779
0.812258	0.054044
0.773334	0.062162
0.732036	0.069843
0.688677	0.076878
0.643641	0.083188
0.597365	0.088633
0.550283	0.093107
0.502833	0.096508
0.455456	0.098771
0.408592	0.099831
0.362664	0.099657
0.318084	0.098229
0.275244	0.095567
0.234523	0.091702
0.196266	0.086685
0.160787	0.080586
0.128359	0.073522
0.099240	0.065625
0.073637	0.057048
0.051734	0.047969
0.033658	0.038587
0.019531	0.029116
0.009363	0.019681

x/c	y/c
0.002994	0.010558
0.000137	0.002224
0.000542	-0.004557
0.004682	-0.008082
0.013924	-0.008145
0.028974	-0.005642
0.049686	-0.000761
0.075990	0.006427
0.107788	0.015924
0.145283	0.028218
0.189738	0.043326
0.242333	0.059055
0.302177	0.072625
0.367054	0.082590
0.434779	0.088528
0.503519	0.090416
0.571672	0.088465
0.637492	0.082748
0.699204	0.074205
0.755903	0.064233
0.807256	0.053686
0.853012	0.043117
0.892933	0.032868
0.926572	0.023228
0.953623	0.014814
0.974197	0.008158
0.988605	0.003516
0.997156	0.000856
1.000000	0.000000

AS6099

$C_{m,c/4} = -0.26$, 6%

x/c	y/c
0.997150	0.000935
0.988846	0.003802
0.975607	0.008529
0.957955	0.014773
0.936275	0.022039
0.910746	0.029800
0.881366	0.037737
0.848281	0.045809
0.811881	0.053946
0.772598	0.061978
0.730866	0.069713
0.687104	0.076947
0.641740	0.083519
0.595210	0.089269
0.547959	0.094068
0.500432	0.097790
0.453065	0.100342
0.406288	0.101645
0.360516	0.101650
0.316147	0.100320
0.273555	0.097663
0.233094	0.093705
0.195083	0.088512
0.159823	0.082173
0.127583	0.074820
0.098612	0.066597
0.073116	0.057676
0.051277	0.048257
0.033235	0.038562
0.019122	0.028835
0.009002	0.019217
0.002736	0.009956
0.000068	0.001548
0.000723	-0.005163
0.005759	-0.008780
0.016321	-0.009560
0.032283	-0.008323
0.053528	-0.005002
0.079881	0.000393
0.111226	0.008171
0.147898	0.018765
0.190889	0.032060
0.241016	0.046467
0.297732	0.059966
0.359630	0.071367
0.425265	0.079902
0.493202	0.085013
0.562049	0.086225
0.629614	0.082637
0.693170	0.075047
0.751400	0.065497
0.804020	0.055054
0.850804	0.044400
0.891534	0.033937
0.925768	0.024018
0.953208	0.015318
0.974010	0.008430
0.988536	0.003628
0.997142	0.000882
1.000000	0.000000